Appl Phys B (2010) 99: 701–707
DOI 10.1007/s00340-010-3921-1

Applied Physics B
Lasers and Optics

Photo electromotive force in CdTe:Ge: manifestation of two photorefractive centers

T.O. dos Santos · J. Frejlich · K. Shcherbin

Received: 9 October 2009 / Revised version: 6 January 2010 / Published online: 2 March 2010
© Springer-Verlag 2010

Abstract The photo-electromotive-force effect in CdTe:Ge is studied. A nontrivial frequency response with two different cutoff frequencies is found in the sample studied when exposed to 1064 nm wavelength. The experimental results reveal that two photorefractive centers with charge carriers of the same sign participate in the space-charge formation. The data for different frequency ranges are analyzed individually in the frame of a one-level model for monopolar semiconductor. The photorefractive centers important at different frequency ranges are associated with two species known for CdTe:Ge. Two values for the diffusion length evaluated from the experimental data are linked to these centers.

1 Introduction

When a photoconductive material is non-homogeneously illuminated, charge carriers are photoexcited in the bright areas and diffuse to the darker ones where they are trapped. In this way the pattern of light is recorded as a spatial electric charge modulation in the material. If the recording pattern of light is put to vibrate, the spatial distribution of photoexcited charge carriers oscillates synchronously. If the oscillation frequency is higher than or comparable to the reciprocal relaxation time of the photoconductor, a stationary space charge field is built up and the photoexcited charge carriers moving in this field produce a photo electromotive force (PEMF) [1]. In a short-circuited sample the ac PEMF current is observed which may be used for the measurement of ultrasonic and acoustic frequencies vibrations as well as for material characterization [1–4].

An interference [2, 3] or a speckle [4–6] pattern of light may be used for PEMF generation and both these techniques have particular advantages. The speckle pattern approach is interesting for practical applications because it requires a very simple setup without any reference beam. Also the speckle PEMF is directly related to transverse vibrations instead of longitudinal ones as is the case for the interference-based setup. The interferometric technique, on the other hand, has the advantages of being described by a simpler mathematical model and of exhibiting a well defined and adjustable pattern of fringes period to be used as reference for measurements, which is not the case for speckle-PEMF.

In the present paper a CdTe:Ge crystal is studied using the interferometric PEMF technique with the $\lambda = 1064$ nm wavelength. It is demonstrated that this sample exhibits a nontrivial frequency response arising from a complicated defect structure. Our experimental data verify that two photorefractive centers with one single type of charge carrier are relevant in this case.

2 Experimental set-up

The studied CdTe:Ge crystal was grown by a modified Bridgman process in Chernivtsy National University, Ukraine. It is rectangular in shape with the dimensions 3.8 mm × 3.5 mm × 7 mm along the [110], [001] and [$1\bar{1}0$] directions, respectively. The faces parallel to ($1\bar{1}0$) and (110) crystallographic planes are optically finished while the side

T.O. dos Santos · J. Frejlich
Instituto de Física "Gleb-Wataghin", UNICAMP, 13083-970
Campinas, São Paulo, Brazil

K. Shcherbin (✉)
Institute of Physics, National Academy of Sciences, Prospekt
Nauki 46, 03028 Kiev, Ukraine
e-mail: kshcherb@iop.kiev.ua
Fax: +380-44-5252359

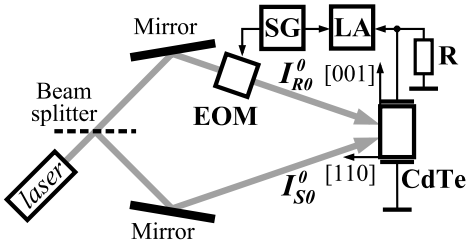

Fig. 1 Experimental set-up: *laser*—Nd^{3+}:YAG laser operating at 1064 nm, *SG*—signal generator, *LA*—lock-in amplifier, *EOM*—electrooptic modulator, *R*—load resistor

faces parallel to the (001) plane are painted with conductive silver glue electrodes.

The experimental set-up is shown schematically in Fig. 1. A single frequency continuous wave Nd^{3+}:YAG laser operating at 1064 nm is the light source. The output laser beam is split into a signal and a reference beams with incident intensities I^0_{S0} and I^0_{R0}, respectively, I_S and I_R representing the intensities of the transmitted beams and I_{S0}, I_{R0} being the respective transmitted intensities in the absence of any hologram. The beam ratio is $\beta = I^0_{S0}/I^0_{R0} \approx 1$. The high visibility of the pattern of fringes in these experiments was chosen in order to improve the signal-to-noise ratio, particularly in PEMF experiments, as the PEMF signal is proportional to the square of the visibility [1, 2]. The grating recording at a high contrast allows, therefore, for the study of PEMF signal with much larger variation of the experimental conditions, such as intensity and grating period. The drawback represented by the generation of higher spatial harmonics for the space-charge field [7] may certainly introduce errors in the evaluation of material parameters like diffusion and Debye lengths. However, small differences in the estimations of material parameters are not significant in this case as we are not concerned about the accurate measurement of parameters but about proving the presence of two different photorefractive centers with different characteristics and one single type of charge carriers.

The recording beams are expanded and directed through the (110)-plane (3.5×7 mm^2 face) into the CdTe:Ge crystal where they interfere to record a space-charge grating. The expanded Gaussian beams have a half-width of intensity distribution of the size of the interelectrode distance, so that they illuminate the whole input face between electrodes with an intensity varying within 50%. An electrooptic modulator EOM driven by a signal generator SG introduces a phase modulation $\Delta\varphi\cos(2\pi f t)$ in the reference beam with amplitude $\Delta\varphi \approx 0.1$ rad and frequency $f(\Omega = 2\pi f)$. The phase modulation produces an oscillation of the interference pattern and gives rise to the PEMF in the crystal. The sample is short-circuited through a 910 Ω load resistor R that is much smaller than the estimated few MΩ for the crystal resistance at the highest intensity $I_0 \approx 160$ mW/cm^2 in the experiments. The voltage from the load resistor is measured by a lock-in amplifier LA at the same modulation frequency f and from these data the first harmonic component of the PEMF photocurrent i^{Ω} is evaluated.

Complementary experiments were also carried out in order to measure the photorefractive two-beam coupling dynamics. The largest interaction length for our sample was used here to increase the signal-to-noise ratio. The crystal was turned by 90° around the [001]-axis (see Fig. 1) so that the $(1\bar{1}0)$-plane became the input face. As in the PEMF experiments, a grating was recorded with the grating vector parallel to the [001] direction, using light polarized perpendicularly to the latter and to the plane of incidence. The handbook electrooptic constant r_{41} is the relevant parameter in this geometry. Shutters placed in front of the crystal allow for blocking/unblocking of both recording beams with a 8 μs switching time. The temporal behavior of the transmitted signal beam I_S was measured after unblocking of the reference beam and vice versa for the dynamics of the reference beam I_R. No phase modulation was used in two-beam coupling experiments.

3 Experimental results

3.1 PEMF frequency response

The frequency response of the PEMF current i^{Ω} with different beam intensities was measured at a grating spacing $\Lambda = 3.3$ μm (spatial frequency $K = 2\pi/\Lambda = 1.9$ μm^{-1}) and reported by dots in Fig. 2. For a simple one-center model of the space-charge formation, the frequency dependence of the PEMF current i^{Ω} should follow the relation [2]

$$i^{\Omega} = i^{\Omega}_0 \frac{2\pi f \tau_{SC}}{\sqrt{1 + (2\pi f \tau_{SC})^2}}, \tag{1}$$

where i^{Ω}_0 is the PEMF current at frequency saturation and τ_{SC} is the characteristic time of the space-charge field formation. It is obvious that the data in Fig. 2 have a more complicated form with a sharp bending around 1 kHz.

The solid lines in Fig. 2 represent the best fit to the experimental data by a simple sum of two relations as in (1) with different amplitudes and time constants ($\tau_1 = 1.1$ ms and $\tau_2 = 12$ μs for the data measured for the largest intensity $I_0 = I^0_{S0} + I^0_{R0} \approx 160$ mW/cm^2). It is evident that two processes with different time constants contribute to the space-charge formation in the studied CdTe:Ge.

3.2 Two-beam coupling dynamics

Similar composite frequency response with two characteristic cutoff frequencies may be observed in a bipolar photoconductor with a long lifetime of one type of carriers (longer

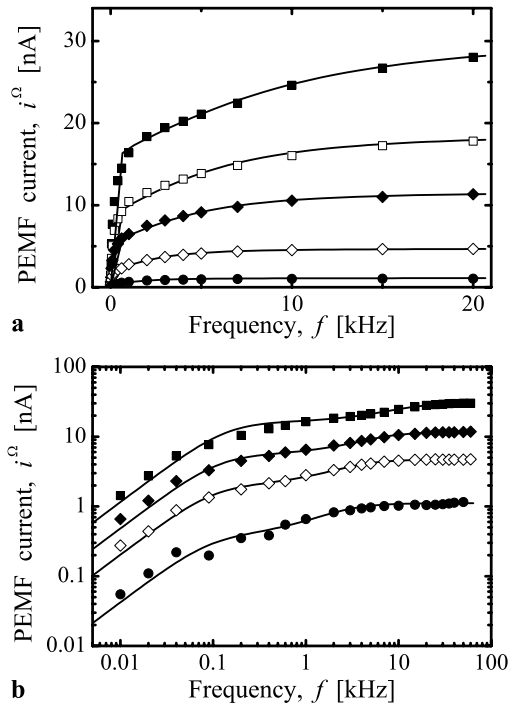

Fig. 2 First harmonic of the PEMF current as a function of modulation frequency in linear (**a**) and log–log (**b**) scale measured at $\Lambda = 3.3$ μm ($K = 1.9$ μm^{-1}) and $I_0 = 160$ mW/cm^2 (■), 106 mW/cm^2 (□), 71 mW/cm^2 (◆), 35 mW/cm^2 (◇), and 14 mW/cm^2 (●). *Solid lines*: best fit by a sum of two equations as (1) with different amplitudes and time constants

than the dielectric relaxation time τ_{di}) and relatively small contribution of these carriers to the photoconductivity (see Fig. 18 in Ref. [1] or Fig. 8 in Ref. [8]). To verify if the studied CdTe:Ge sample exhibits similar properties, the dynamics of two-beam coupling was measured at the same experimental conditions that the PEMF current was measured, with total light intensity $I_0 \approx 160$ mW/cm^2. The temporal behavior of the transmitted signal beam, when the reference beam is unblocked at $t = 0$, is shown in Fig. 3 by squares. The signal beam shows amplification because of the energy transfer on the refractive index grating recorded in the diffusion mode [9]. The unblocking time of our shutters is about 8 μs. This is why we cannot accurately study the dynamics of the signal beam in a short time scale. It is obvious, however, that the intensity increase is not a single exponential but may be described by a sum of two exponential functions of the form

$$\Delta I_S = \Delta I_1\big[1 - \exp(-t/\tau_1)\big] + \Delta I_2\big[1 - \exp(-t/\tau_2)\big]. \quad (2)$$

The best fit by (2) to the experimental gain dynamics in Fig. 3 gives $\tau_1 = 0.45$ ms and $\tau_2 = 28$ μs. These time constants are similar (in order of magnitude) to the corresponding ones evaluated from PEMF current experiments (Fig. 2).

The reference beam behind the crystal shows attenuation when the signal is unblocked, also showing an evolution

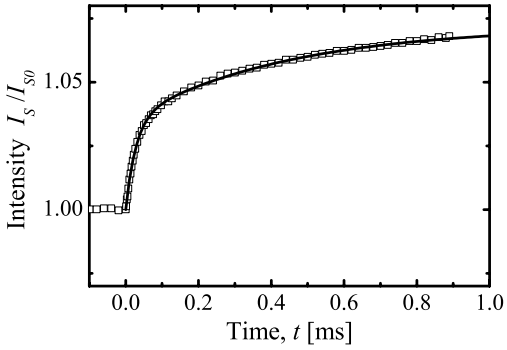

Fig. 3 Temporal behavior of the transmitted signal beam intensity in two-beam coupling at $\Lambda = 3.3$ μm ($K = 1.9$ μm^{-1}) and $I_0 = 160$ mW/cm^2; *squares*: experiment, *solid line* is for the best fit by (2) with $\tau_1 = 0.45$ ms and $\tau_2 = 28$ μs

with two characteristic times similar to those for the case of signal amplification.

Thus, the same two processes with two different time constants manifest themselves in two-beam coupling as well as in PEMF experiments. The additive contribution to the grating formation from these well-separated processes in the two-beam coupling energy transfer indicates that the same charge carriers, without bipolar conductivity, are involved in these two-time constant processes.

The two-step grating formation may occur if photoexcitation of the same charge carriers occurs from two deep centers in the band gap [10–12]. Such complicated behavior is not surprising for CdTe because several centers often participate in the space-charge formation in CdTe:Ge [13, 14] as well as in CdTe:V [15, 16]. It has been demonstrated [10–12] that the overall grating may be considered in some cases as a sum of uncoupled constituent components, each one with a certain amplitude and characteristic time. As the time constants are well separated in our sample, we consider in the following analysis of the PEMF data the overall space-charge grating composed of two uncoupled "fast" and "slow" components and characterize these components independently.

At the same time it should be noted that the frequency response of the PEMF current becomes even more complicated at grating spacing around 9 μm ($K \sim 0.7$ μm^{-1}) where a small but persistent dip is detected at frequency 1–2 kHz as is shown in Fig. 4. We attribute this dip to electron–hole competition, but we do not analyze this feature in detail, because it is observed for a limited range of fringe periods and because it is insignificant as compared to other contributions.

3.3 Charge transport characterization with the PEMF technique

Spectra of PEMF current similar to that shown in Fig. 2 were measured at different grating spacings for different intensi-

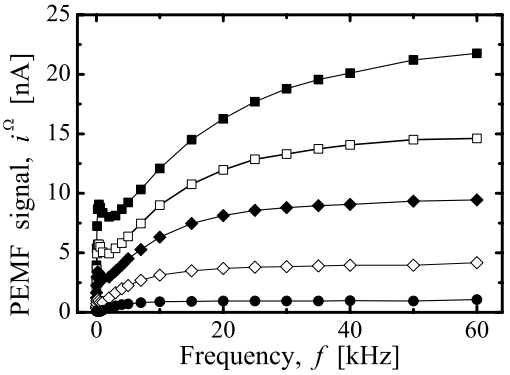

Fig. 4 First harmonic of the PEMF current as a function of modulation frequency measured at $\Lambda = 9$ μm ($K = 0.7$ μm^{-1}) and $I_0 = 160$ mW/cm^2 (■), 106 mW/cm^2 (□), 71 mW/cm^2 (◆), 35 mW/cm^2 (◇), and 14 mW/cm^2 (●). *Solid lines* guide to eyes

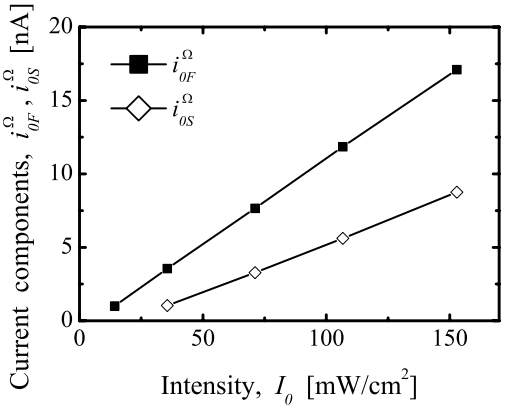

Fig. 5 Amplitudes of the fast (i^{Ω}_{0F}) and slow (i^{Ω}_{0S}) components of the PEMF current as a function of intensity measured at $\Lambda = 9$ μm ($K = 0.7$ μm^{-1})

ties. The amplitude i^{Ω}_{0S} and the time constant τ_S of the slow component of the PEMF current are evaluated from the low frequency region below 1 kHz of the collected experimental spectra while for evaluation of the characteristics i^{Ω}_{0F} and τ_F for the fast component the high frequency range above 1 kHz is used.

The first harmonic amplitude of the fast component of the PEMF current as a function of intensity evaluated from the spectra measured at $\Lambda = 9$ μm ($K = 0.7$ μm^{-1}) is shown by solid squares in Fig. 5 whereas the slow component is shown by open diamonds in this figure. Both components increase with intensity showing a linear growth starting from nonzero intensity, at which the corresponding component of the space-charge grating saturates in intensity. This behavior for every component is in agreement with the theory for one-level model [1], which links the linear dependence of the PEMF current amplitude to the linear growth of the photoconductivity with intensity. The linearity of the dependences in Fig. 5 suggests that there is no considerable charge transfer between the two species participating in the grating formation. Otherwise a nonlinear dependence of photoconductivity should distort the linear shape of the dependences in Fig. 5 [17].

The characteristic time of the space-charge grating is inversely proportional to the conductivity [18]:

$$\tau_{\mathrm{SC}} \propto \tau_{\mathrm{di}} = \frac{\varepsilon\varepsilon_0}{\sigma_D + \sigma_P} = \frac{\varepsilon\varepsilon_0}{\sigma_D + \kappa I}, \tag{3}$$

where τ_{di} is the dielectric relaxation time of the material, ε and ε_0 are the dielectric permittivity of the material and free space, respectively, σ_D and σ_P are the dark and photoconductivity, κ is the specific photoconductivity. The reciprocal time constant for the fast grating estimated from experimental spectra measured at $\Lambda = 9$ μm ($K = 0.7$ μm^{-1}) are shown in Fig. 6a while Fig. 6b represents the data associated with the slow grating. One can see that the time constant of the slow process has a considerably weaker dependence on

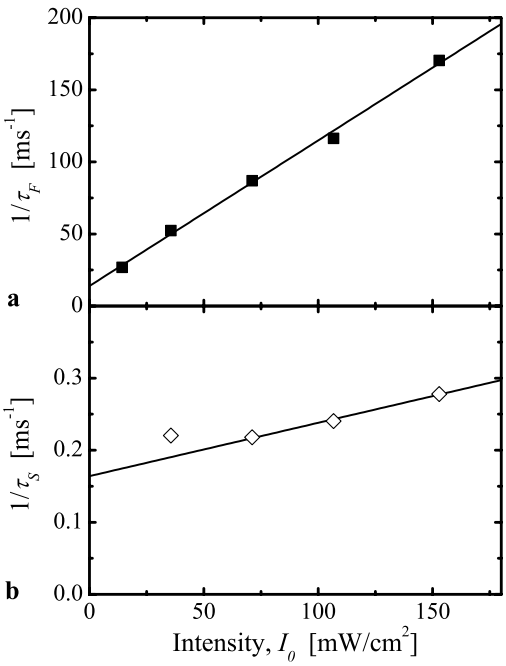

Fig. 6 Reciprocal relaxation time of the fast (**a**) and slow (**b**) components of the grating as a function of intensity measured at $\Lambda = 9$ μm ($K = 0.7$ μm^{-1})

intensity than the fast one. Therefore photoactive centers associated with the slow grating give a much smaller contribution to the photoconductivity in the studied CdTe:Ge crystal.

The grating response time approaches the dielectric relaxation time at a large grating spacing [18] and proportionality sign may be replaced in (3) by equality sign. The grating spacing $\Lambda = 9$ μm was chosen in this case because it is the largest grating spacing at which the signal for both, slow and fast, components of the PEMF current is large enough for accurate measurement of the time constants over the whole intensity range. Assuming that the time constant is close to the dielectric time constant at this grating spacing,

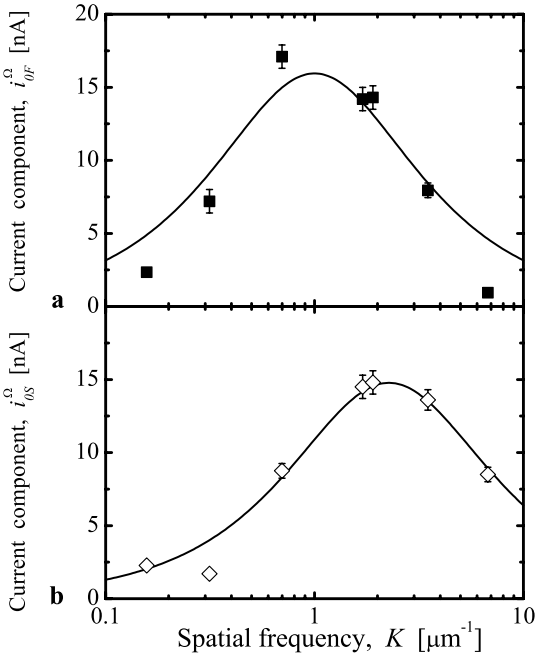

Fig. 7 Amplitudes of the fast (**a**) and slow (**b**) components of the PEMF current as a function of spatial frequency (*dots*) measured for $I_0 \approx 160$ mW/cm^2. The *solid lines* are for the best fit of (4) with $L_D^F = 1$ μm (**a**) and $L_D^S = 0.44$ μm (**b**)

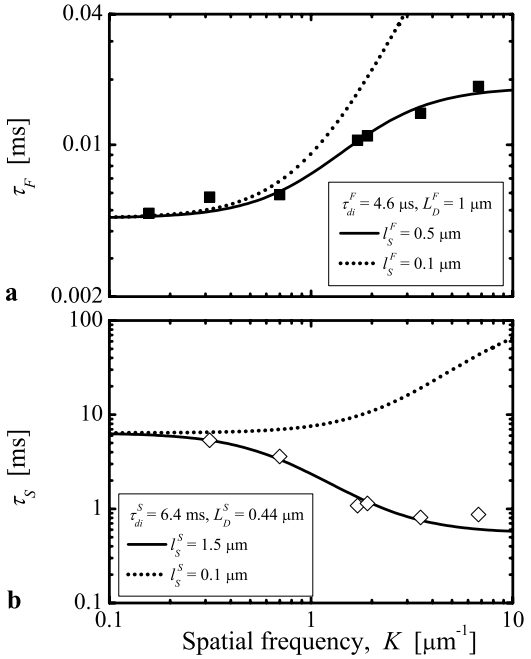

Fig. 8 Time constants of the fast (**a**) and slow (**b**) components of the space-charge grating as a function of spatial frequency (*dots*) measured for $I_0 \approx 160$ mW/cm^2. The *solid lines* are for the best fit of (5) with (**a**): $L_D^F = 1$ μm, $\tau_{\rm di}^F = 4.6$ μs, $l_S^F = 0.5$ μm, and (**b**): $L_D^S = 0.44$ μm, $\tau_{\rm di}^S = 6.4$ ms, $l_S^S = 1.5$ μm. *Dotted lines* are for the calculations according (5) with the same values of L_D^F, $\tau_{\rm di}^F$, L_D^S and $\tau_{\rm di}^S$ as for the *solid lines* and with $l_S^F = 0.1$ μm (**a**) and $l_S^S = 0.1$ μm (**b**)

the contributions of the slow and fast processes of the charge redistribution to the overall dark conductivity and specific conductivity may be estimated from a linear fit of (3) to the data of Fig. 6. The fit gives $\sigma_{\rm DS} = 1.4 \times 10^{-10}$ $(\Omega \times {\rm cm})^{-1}$, $\kappa_S = 6.4 \times 10^{-6}$ cm/($\Omega \times$ W) and $\sigma_{\rm DF} = 1.2 \times 10^{-8}$ $(\Omega \times {\rm cm})^{-1}$, $\kappa_F = 8.7 \times 10^{-5}$ cm/($\Omega \times$ W) for the contributions from the slow and fast processes, respectively.

For a simple one-level model of the space-charge formation with no traps saturation the amplitude of the PEMF current depends on spatial frequency as [1]

$$i^{\Omega} \propto \frac{K}{1 + K^2 L_D^2}, \tag{4}$$

where $L_D = \sqrt{\mu \tau k T / e}$ is the diffusion length, μ is the mobility and τ is the lifetime of photoexcited carriers and e is the value of the electron charge. The spatial frequency dependences of the PEMF current amplitude measured at intensity $I_0 = 160$ mW/cm^2 are shown by dots in Fig. 7a for the fast (i_{0F}^{Ω}) and in Fig. 7b for the slow (i_{0S}^{Ω}) component. The dependences exhibit a bell-shaped profile in a logarithmic scale with maximum at optimal spatial frequency $K_{\rm opt} = 1/L_D$. The solid lines represent the best fit to the experimental data by (4) with $L_D^F = 1$ μm for the fast and $L_D^S = 0.44$ μm for the slow grating. The presence of two different diffusion lengths for the same charge carriers means that a part of the charge carriers diffuse by a length L_D^F before being captured by species of one type while the rest of the charge carriers diffuse by L_D^S before being captured by other traps. The mobility-lifetime product associated with these diffusion lengths can be calculated $\mu\tau^F \approx 4 \times 10^{-7}$ cm^2/V for the fast process and $\mu\tau^S \approx 7.5 \times 10^{-8}$ cm^2/V for the slow process. As the mobility is the same for the same charge carriers we can conclude that the ratio of the lifetime of carriers captured by different centers is $\tau^F/\tau^S \approx 5.3$.

The space-charge grating time constant depends on spatial frequency as [1, 18]

$$\tau_{\rm SC} = \tau_{\rm di} \frac{(1 + K^2 L_D^2)}{(1 + K^2 l_S^2)}, \tag{5}$$

where l_S is the Debye screening length: $l_S^2 = (\varepsilon \varepsilon_0 k_B T)/(e^2 N_{\rm eff})$, k_B is the Boltzmann constant, T is the absolute temperature, and $N_{\rm eff}$ is the effective trap density. The time constants evaluated from the PEMF current spectra measured at different spatial frequencies for $I_0 \approx 160$ mW/cm^2 are represented by dots in Fig. 8a for the fast and in Fig. 8b for the slow components of the overall space-charge grating. The fast time constant component of the grating grows monotonously with spatial frequency. Such a behavior is typical for semiconductors and sillenites (see, e.g. [19, 20]), in which the diffusion length is larger than the Debye screen-

ing length ($L_D > l_S$), as one can see from (5). The time constant of the slow component, however, decreases with spatial frequency. Such a decrease of τ_{SC} with K is observed in materials where ($L_D < l_S$) and is typical for ferroelectrics such as $LiNbO_3$ [19].

The solid lines in Fig. 8 represent the best fit to the experimental data by (5) with $l_S^F = 0.5$ μm, $\tau_{di}^F = 4.6$ μs for the fast and $l_S^S = 1.5$ μm, $\tau_{di}^S = 6.4$ ms for the slow component of the grating, and with the diffusion lengths evaluated previously from the spatial frequency dependences of the amplitudes of the current components (Fig. 7). The large (three orders of magnitude) difference between the dielectric time constants of the fast and slow components is a clear indication that at least two different charge transfer processes through different traps are here involved.

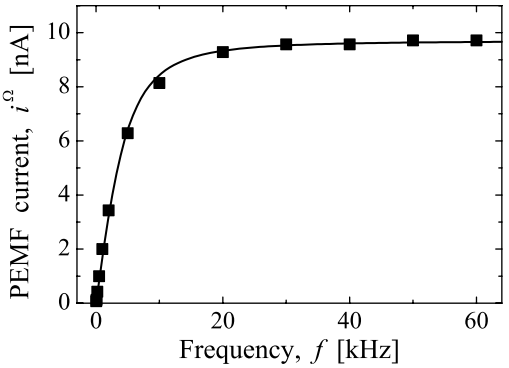

Fig. 9 First harmonic of the PEMF current as a function of modulation frequency measured at $\lambda = 1550$ nm, $\Lambda = 40$ μm ($K \approx 0.16$ μm^{-1}) and $I_0 = 80$ mW/cm^2 (*dots*). The *solid line* is for the best fit of (1) with $\tau_{SC} = 28$ μs

4 Discussion

The theoretical fit of experimental data from PEMF and two-wave mixing experiments clearly show that at least two different (a fast and a slow) photoactive centers inside the band gap do participate in charge transport in CdTe:Ge. Results from two-wave mixing suggest that charge carriers from both photoactive centers are of the same sign whereas PEMF experiments show that there is no much coupling between both species. Diffusion and Debye lengths were estimated respectively to be 0.44 μm and 1.5 μm for the slow and 1 μm and 0.5 μm for the fast species whereas the fast-to-slow lifetime carriers ratio was found to be $\tau^F/\tau^S = 5.3$.

At the same time the present sample shows an efficient two-beam coupling at small grating spacing (large K) and even at the reflection geometry, because the crystal exhibits a large effective trap density, which has been estimated to be about $N_{eff} \approx 2.4 \times 10^{16}$ cm^{-3} for $\lambda = 1064$ nm [21].

With our definition of the Debye screening length (which is 2π different from the definition used in [21]) this concentration corresponds to $l_S \approx 0.024$ μm, which is much smaller than the estimation from the experimental data of Fig. 8 with fit by (5). The trap density estimated in Ref. [21] from two-beam coupling experiments corresponds to a sum of concentrations of the centers responsible for the slow and fast gratings. Therefore, the concentration of each center is smaller (each relative Debye screening length is larger) than the value estimated in Ref. [21]. The dotted lines in Fig. 8 represent the calculation according (5) with $l_S^F = 0.1$ μm, $l_S^S = 0.1$ μm with the other parameters remaining the same as for the solid lines. It is evident that the experimental data cannot be described with such low values. It should be noted that the calculation according (5) gives almost the same results in the studied spatial frequency range for any $l_S^F \leq 0.1$ μm, $l_S^S \leq 0.1$ μm with other parameters kept the same. Effective two-beam coupling at the reflection geometry clearly demonstrates that the Debye screening length is really smaller than 0.1 μm. The disagreement in the estimation for the Debye screening length suggests that a more complicated model should be developed for an accurate explanation of the spatial frequency dependences of the time constants. At the same time the dependences are well described qualitatively with individual analysis of two components in the frame of the one-species model with (5).

It should be noted that only some of the CdTe:Ge samples that were tested exhibit a complicated frequency response of the PEMF current at 1064 nm as presented in Figs. 2, 4. The other samples demonstrate single-component spectra similar to the fast component in the studied sample. Moreover, excitation at $\lambda = 1550$ nm, even for the present sample, shows a monotonic frequency response as seen by dots in Fig. 9 for a grating period $\Lambda = 40$ μm ($K = 0.16$ μm^{-1}) and $I = 80$ mW/cm^2 with the solid line representing the best data fit by (1) with a time constant $\tau_{SC} = 28$ μs without evidence of another photoactive species. It is clear that only one space-charge grating remains important at $\lambda = 1550$ nm where its microsecond range response time suggests that this grating corresponds to the fast grating at $\lambda = 1064$ nm excitation. It is evident, therefore, that the characteristic features such as complicated PEMF spectrum and two-exponentional dynamics of the two-beam coupling are determined mainly by crystal properties, but not by the experimental conditions such as, for example, a high contrast of the interference fringes, which may lead to a strong nonlinearity of the grating formation (see e.g. [7]).

The energy level diagram describing the photoinduced charge transfer processes in CdTe:Ge has been already reported elsewhere [14] and is shown in Fig. 10. The holes are responsible for grating recording at 1064 nm (photon energy $h\nu = 1.17$ eV) [14, 22]. They are photoexcited from ionized Ge on Cd site (Ge^+) and from a not fully characterized center X in a neutral state (X^0), which are characterized by broad absorption bands with a half-width about 0.15–0.2 eV even at the liquid helium temperature $T = 4.3$ K [14, 22].

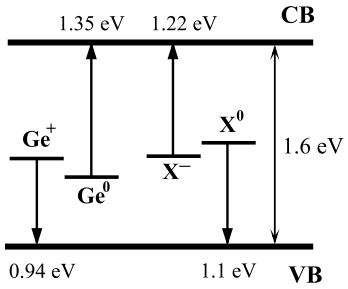

Fig. 10 The energy level diagram describing photoexcitations in photorefractive CdTe:Ge

Only the center Ge^+ with photoionization energy 0.94 eV remains important for excitation at 1550 nm ($h\nu = 0.8$ eV). Therefore we can associate the fast process detected both at $\lambda = 1064$ nm and at $\lambda = 1550$ nm with the species Ge^+. Consequently the slow grating only detected at $\lambda = 1064$ nm should be also a hole-based one and attributed to the center X in a neutral (X^0) state. The absence of the slow grating in some CdTe:Ge samples at $\lambda = 1064$ nm indicates that species X^0 is not necessarily present in a relevant concentration in all CdTe:Ge crystals.

5 Conclusions

In the present paper it is demonstrated that two different processes associated with the charge transport of carriers of the same type through different trap species may contribute to the space-charge formation in a photoconductive CdTe:Ge crystal. The time constants of these processes differ by two orders of magnitude in the sample under study. A simple model considering the formation of two independent gratings adequately explains our experimental results qualitatively and allows for characterization of the charge transport associated with the different species. Experimental inconsistencies of the results involving Debye lengths may indicate, however, that the model with uncoupled single charge carrier with two different photorefractive centers may be more complex than that.

The present results do explain the relatively small photo-to-dark conductivity ratio and the rather slow response of this CdTe:Ge crystal sample that were found in our previous work [6] using speckle PEMF techniques in a low frequency range that were unexpected for a photosensitive semiconductor crystal.

The presently detailed characterization in the high frequency domain allows one to identify the charge transport linked to the fast and the slow components of the space-charge grating which are unambiguously associated with known photorefractive centers in the CdTe:Ge crystal.

Acknowledgements This research was partially supported by Fundação de Amparo à Pesquisa do Estado de São Paulo, Brazil (FAPESP), Conselho Nacional de Desenvolvimento Científico e Tecnológico (CNPq, Brazil). K. Shcherbin cordially thanks colleagues from Laboratorio de Optica, IFGW-UNICAMP for their hospitality. The CdTe:Ge crystal was provided by Z. Zakharuk and I. Rarenko.

References

1. S. Stepanov, in *Handbook of Advanced Electronic and Photonic Materials and Devices*, vol. 2, ed. by H.S. Nalwa (Academic Press, New York, 2001), p. 205
2. S.I. Stepanov, I.A. Sokolov, G.S. Trofimov, V.I. Vlad, D. Popa, I. Apostol, Opt. Lett. **15**, 1239 (1990)
3. I.A. Sokolov, S.I. Stepanov, G.S. Trofimov, J. Opt. Soc. Am. B **9**, 173 (1992)
4. N.A. Korneev, S.I. Stepanov, J. Mod. Opt. **38**, 2153 (1991)
5. L. Mosquera, J. Frejlich, J. Opt. A, Pure Appl. **6**, 1001 (2004)
6. T.O. dos Santos, J. Frejlich, J.C. Launay, K. Shcherbin, Appl. Phys. B **95**, 627 (2009)
7. E. Serrano, V. López, M. Carrascosa, F. Agulló-López, J. Opt. Soc. Am. B **11**, 670 (1994)
8. N.A. Korneev, S.S. Mansurova, S.I. Stepanov, T.J. Hall, A.K. Powell, J. Opt. Soc. Am. B **13**, 2278 (1996)
9. N.V. Kukhtarev, V.B. Markov, S.G. Odulov, M.S. Soskin, V.L. Vinetskii, Ferroelectrics **22**, 961 (1979)
10. G.C. Valley, Appl. Opt. **22**, 3160 (1983)
11. M. Carrascosa, F. Agullo-Lopez, Appl. Opt. **27**, 2851 (1988)
12. M.C. Bashaw, M. Jeganathan, L. Hesselink, J. Opt. Soc. Am. B **11**, 1743 (1994)
13. B. Briat, K. Shcherbin, B. Farid, F. Ramaz, Opt. Commun. **156**, 337 (1998)
14. B. Briat, F. Ramaz, B. Farid, K. Shcherbin, H.J. von Bardeleben, J. Cryst. Growth **197**, 724 (1999)
15. L.A. de Montmorillon, Ph. Delaye, G. Roosen, H. Bou Rjeily, F. Ramaz, B. Briat, J.G. Gies, J.P. Zielinger, M. Tapiero, H.J. von Bardeleben, T. Arnoux, J.C. Launay, J. Opt. Soc. Am. B **13**, 2341 (1996)
16. Ph. Delaye, L.A. de Montmorillon, I. Biaggio, J.C. Launay, G. Roosen, Opt. Commun. **134**, 580 (1997)
17. D. Mahgerefteh, J. Feinberg, Phys. Rev. Lett. **64**, 2195 (1990)
18. J. Frejlich, *Photorefractive Materials* (Wiley, New York, 2006)
19. R.A. Mullen, in *Photorefractive Materials and Their Applications*, vol. 1, ed. by P. Gunter, J.-P. Hugard (Springer, Berlin, 1988), pp. 167
20. K. Shcherbin, A. Shumelyuk, S. Odoulov, P. Fochuk, G. Brost, SPIE Proc. **2795**, 236 (1996)
21. K. Shcherbin, Appl. Opt. **48**, 371 (2009)
22. K. Shcherbin, S. Odoulov, F. Ramaz, B. Farid, B. Briat, H.J. von Bardeleben, Ph. Delaye, G. Roosen, Opt. Mater. **18**, 151 (2001)